Responses of mesosphere and lower thermosphere temperatures to gravity wave forcing during stratospheric sudden warming

Chihoko Yamashita,[1,2] Han-Li Liu,[1] and Xinzhao Chu[2]

Received 4 January 2010; revised 29 March 2010; accepted 2 April 2010; published 6 May 2010.

[1] We examine the responses of the mesosphere and lower thermosphere (MLT) temperatures to gravity waves (GWs) during stratospheric sudden warming (SSW) using TIME-GCM through modifying GW parameters. Our study confirms that the height of GW forcing region is mainly determined by GW amplitude and wavelength, and its vertical depth is closely tied to the spectral width of GW phase speed. The GW forcing controls the pattern and strength of residual circulation and thereby the characteristics of the MLT cooling and warming regions. The planetary wave (PW) forcing in the MLT also affects the vertical depth and magnitude of MLT temperature anomalies through further modifying the residual circulation. These PWs in MLT are likely generated in-situ by the GW forcing at high latitudes. Therefore, the mechanisms of GW controlling the MLT temperature during a SSW are directly through GW forcing and indirectly through generating PWs in-situ.
Citation: Yamashita, C., H.-L. Liu, and X. Chu (2010), Responses of mesosphere and lower thermosphere temperatures to gravity wave forcing during stratospheric sudden warming, *Geophys. Res. Lett.*, *37*, L09803, doi:10.1029/2009GL042351.

1. Introduction

[2] Stratospheric sudden warmings (SSWs) have significant impacts on global atmospheric circulation in the stratosphere, mesosphere, and thermosphere [e.g., *Matsuno*, 1971; *Labitzke*, 1972; *Liu and Roble*, 2002]. Sudden enhancement of planetary waves (PWs) and their interactions with the mean flow are widely accepted as the cause of SSWs [*Matsuno*, 1971]. Associated with SSWs, cooling in the mesosphere and warming in the lower thermosphere have been observed [e.g., *Labitzke*, 1972; *Siskind et al.*, 2005; *Coy et al.*, 2005]. These MLT temperature anomalies are most likely caused by changes in filtering of gravity waves (GWs) due to wind reversal [*Holton*, 1983; *Liu and Roble*, 2002]. During SSWs, GW forcing changes from westward to eastward at middle and high latitudes and induce an equatorward flow in the upper mesosphere. Such flow drives upward circulation in the mesosphere and downward circulation in the lower thermosphere, resulting in adiabatic cooling and warming in the mesosphere and lower thermosphere, respectively [*Liu and Roble*, 2002].

[3] These MLT temperature anomalies associated with SSWs are captured by the Thermosphere-Ionosphere-Mesosphere-Electrodynamics General Circulation Model (TIME-GCM), the Navy-Operational Global Atmospheric Prediction System - Advanced Level Physics and High Altitude (NOGAPS-ALPHA), and the Canadian Middle Atmosphere Model Data Assimilation System (CMAM-DAS) [*Liu and Roble*, 2002; *Coy et al.*, 2005; *Ren et al.*, 2008]. The importance of GW forcing for capturing MLT cooling has been examined using the NOGAPS-ALPHA model with and without Rayleigh friction and the CMAM-DAS model with and without a non-orographic GW parameterization [*Coy et al.*, 2005; *Ren et al.*, 2008]. In general, simulations with GWs considered gave more realistic results in the MLT region than without the parameterization. However, discrepancies still exist between simulations and observations in the height, vertical depth, and magnitude of the cooling and warming regions [*Siskind et al.*, 2005; *Coy et al.*, 2005; *Liu and Roble*, 2002]. For example, the mesospheric cooling region in the Sounding of the Atmosphere using Broadband Emission Radiometry (SABER) observations for the 2002 Southern Hemisphere SSW is narrower and lower than in TIME-GCM simulations, while the mesospheric cooling region is much wider during the 2008 Northern Hemisphere (NH) SSW in SABER. Furthermore, the characteristics of the MLT temperature anomalies also vary from event to event. Because of the crucial role of GW forcing in MLT dynamics, both the model-observation discrepancy and the variability of the MLT response are likely tied to GWs for their parameterization in models [*Coy et al.*, 2005; *Ren et al.*, 2008] and their variability in different SSW events. It is thus necessary to systematically quantify the dependence of the MLT temperature responses to SSWs on the GW parameters, which is the primary goal of the current work. In addition, we examine the role of PWs generated in-situ by GW forcing in the MLT. The generation of these PWs was discussed by *Smith* [1996], but their roles in the MLT temperature responses to SSWs have not been fully examined. The numerical tool used for this study is the NCAR (National Center for Atmospheric Research) TIME-GCM, which has a unique advantage of an upper boundary at ~500 km, thus the capability of simulating thermospheric effects.

2. Model and the 2008 SSW in Northern Hemisphere

[4] The TIME-GCM developed at the NCAR is used for this study. The horizontal resolution is 2.5° × 2.5° (latitude × longitude), and the vertical resolution is four grid points per scale height. The lower boundary is specified by the European Centre for Medium-Range Weather Forecasts (ECMWF) data at 10 hPa every 6 hours, and the model domain is ~500 km with 89 vertical levels. Detailed descriptions of

[1]High Altitude Observatory, National Center for Atmospheric Research, Boulder, Colorado, USA.
[2]Cooperative Institute for Research in Environmental Sciences and Department of Aerospace Engineering Sciences, University of Colorado at Boulder, Boulder, Colorado, USA.

0094-8276/10/2009GL042351

Table 1. GW Parameters Used in GW Parameterization

	Range of Phase Velocities[a] (m/s)	Horizontal Wavelength (km)	Momentum Flux (Pa)
Base Case	−90 to +90	100	$\sim 1 \times 10^{-5}$
Case 1	−30 to +30	100	$\sim 1 \times 10^{-5}$
Case 2	−90 to +90	1000	$\sim 1 \times 10^{-4}$

[a]Spectral width.

TIME-GCM are provided by *Liu and Roble* [2002] and references therein. TIME-GCM employs a GW parameterization based on a linear saturation theory [*Lindzen*, 1981]. GW input is specified at 10 hPa with a discrete spectrum (15 m/s interval) in Gaussian shape. The spectral width (defined as the range of phase velocity), horizontal wavelength, and wave amplitude are varied in the parameterization scheme, and the parameters used in this study are summarized in Table 1. Here, we use a fixed Gaussian distribution with its spectral center at ~25 m/s and FWHM (full width at half maximum) of ~80 m/s, and then truncate two wings to take the middle portion of ±30 or ±90 m/s for this study. In all cases of simulations, we vary GW parameters only from 0° to 90°N while keeping the base case parameters for 0° to 90°S.

[5] Minor and major warmings were observed in the NH in 2008. The episode of the minor SSW event from January 18 to January 29 is used for this study. In Figure 1, the color contours are the zonal mean temperature anomalies, which are defined as the differences between each day temperature and the temperature before the 2008 SSW on January 18. Figures 1a and 1b (remaining plots in Figure 1 will be used for later discussion) show SABER (Version 1.07) observation and the base case TIME-GCM simulation, respectively. The base case TIME-GCM captures the general features of these observed temperature anomalies; however, it does not reproduce some detailed observed features, e.g., the lower thermospheric warming in TIME-GCM is significantly stronger than in SABER, while the height and vertical depth of the simulated mesospheric cooling are higher and narrower, respectively, than observed by SABER. It should be noted that the main purpose of the current study is not to reproduce the exact observed features, but to use this event as a test bed to study how the MLT temperature responds to different GW parameters in TIME-GCM during SSWs.

3. Analysis Results

3.1. Profile Study Using Gravity Wave Parameterization Scheme

[6] We examine how GW forcing varies with different GW parameters input to the parameterization scheme. Figures 2a and 2b show forcing generated by GWs with different spectral widths and horizontal wavelengths using the wind profile plotted in Figure 2c during a SSW at high latitudes. In Figure 2a, the GW forcing region expands upward by ~15 km when the spectral width is increased from ±30 m/s to ±90 m/s with a constant horizontal wavelength of 100 km. This upward expansion is caused by faster GWs propagating to and breaking at higher altitudes. The magnitude of total GW forcing also increases with the wider spectral width as more wave components are introduced. In Figure 2b, the horizontal wavelength of input GWs is varied from 1000 km to 10 km with a constant spectral width of ±90 m/s. As the horizontal wavelength decreases, GW forcing becomes stronger, the forcing region expands, and

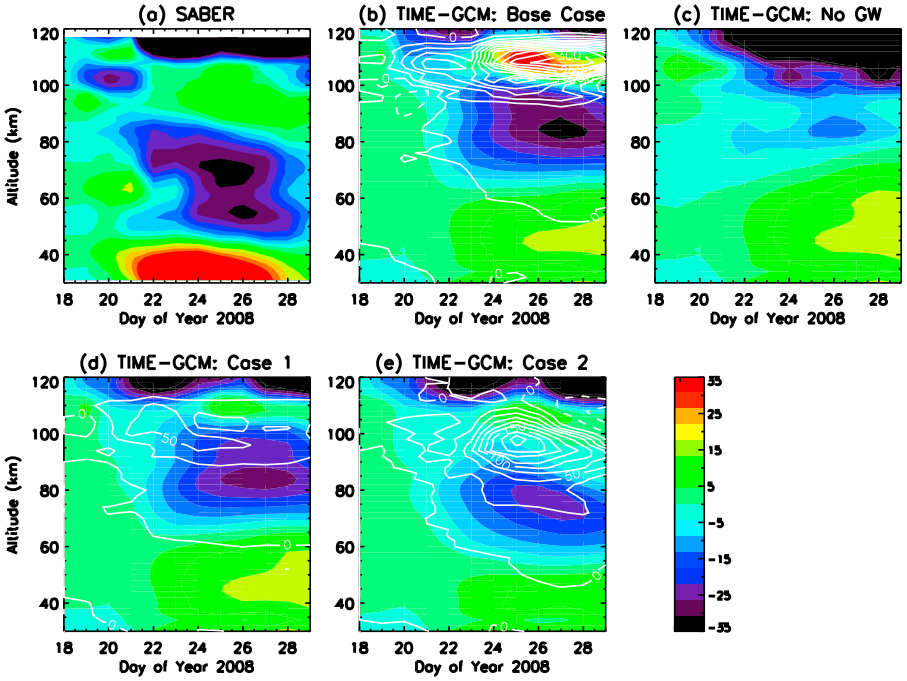

Figure 1. (a) SABER observations at 80°N ± 2.5° and TIME-GCM simulations at 81.25°N with different GW parameters: (b) no GW parameterization, (c) base case, (d) case 1, and (e) case 2. Color contours show the zonal mean temperature anomalies (K) at 12UT after day 18, 2008. Line contours show the zonal mean GW forcing changes (m/s/day) at 12UT. Solid/dashed lines represent the eastward/westward forcing, respectively.

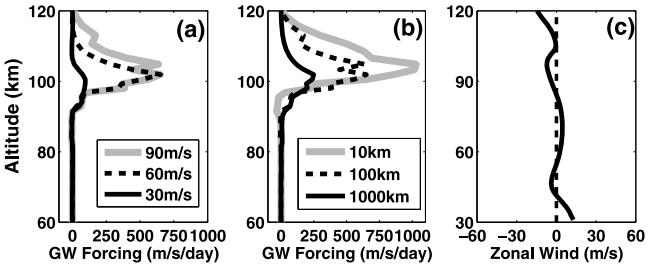

Figure 2. GW forcing output from the GW parameterization. (a) Varying spectral range of ±90 m/s (thick gray), ±60 m/s (dashed), and ±30 m/s (black solid) with a constant horizontal wavelength of 100 km and (b) setting the horizontal wavelength to 10 km (thick gray), 100 km (dashed), and 1000 km (black solid) with a constant spectral range of ±90 m/s. Figures 2a and 2b show GW forcing calculated under (c) the zonal wind condition.

the altitude of the maximum GW forcing increases. This is because the dispersion relations dictate that for a fixed phase speed, GWs with shorter horizontal wavelengths have higher frequencies and longer vertical wavelengths, and these waves can propagate to higher altitudes [*Holton*, 1983]. No strong forcing is observed above the height of ~100 km in the 1000 km case (Figure 2b) as the breaking altitudes of these waves are lower than other cases.

3.2. Temperature Anomaly in TIME-GCM

[7] Equipped with the understanding from Section 3.1, we now examine how the MLT cooling and warming regions respond to GW forcing in TIME-GCM. Figures 1b–1e show TIME-GCM simulations for 4 different cases: A case without GW parameterization and three cases with GWs as listed in Table 1. Compared with the base case, case 1 uses the narrower spectral width and case 2 uses the longer horizontal wavelength and larger amplitude GWs. In Figure 1c for the case without the GW parameterization, no warming occurs in the lower thermosphere but there are ~17 K stratospheric warming and ~10 K mesospheric cooling. Compared to Figure 1c (no GWs), the base case (Figure 1b) gives a similar magnitude of stratospheric warming, but much stronger cooling (~30 K) in the mesosphere and warming (~29 K) in the lower thermosphere. In case 1 (Figure 1d), the mesospheric cooling and lower thermospheric warming are weaker by ~4 K and ~22 K, respectively, than the base case. Case 2 (Figure 1e) has the height and magnitude of the mesospheric cooling region to be ~10 km lower and ~9 K weaker, respectively, than the base case. In case 2, GWs break at lower altitudes, thereby damping PWs in the breaking region. This prevents the PWs from growing to larger amplitudes thus resulting in a weaker, lower, and narrower warming region below 70 km compared to the base case. Although GWs have some influence on the characteristics of warming below 70 km, the stratospheric warming below 70 km and stratospheric jet reversal (not shown) occur in all cases of TIME-GCM simulations with and without GW parameterization, confirming that PWs are the main driver of SSWs [*Matsuno*, 1971]. Nevertheless, the magnitude, height, and vertical depth of the cooling and warming regions in the MLT vary significantly with different GW forcing.

3.3. Residual Circulation Induced by GW and PW Forcings

[8] The changes of GW forcing during this SSW relative to January 18 are over-plotted as white line contours on Figures 1b–1e. The vertical depth of GW forcing region is wider in the base case than in case 1, because the base case uses the wider range of GW spectrum. Moreover, the height of GW forcing region is lower in case 2 than the base case due to the longer horizontal wavelength and lager amplitude GWs used in case 2. These results are consistent with the trend shown in Section 3.1 and the results presented by *Holton* [1983].

[9] Now we investigate the mechanisms how GW forcing affects the height, vertical depth, and magnitude of the cooling and warming regions in the MLT. The lower thermospheric warming and the mesospheric cooling occur above and below the peak eastward forcing region, respectively, in Figures 1d and 1e. Compared to Figure 1b, the heights of GW forcing in Figure 1e are lower by ~10 km, and the heights of the cooling and warming regions are also lower by ~10 km. The magnitudes of warming at 100–120 km and cooling at 70–100 km in the base case are much stronger than those in case 1 and case 2, because the larger changes of eastward GW forcing in the base case induce stronger upward/downward circulation in the MLT than in other cases. The vertical depth of the cooling regions in case 2 is larger than in case 1 as eastward GW forcing region is wider in case 2. Therefore, the height, vertical depth, and magnitude of the MLT cooling and warming regions generally agree with the characteristics of GW forcing regions. However, the following exceptions are noted. First, the magnitudes of GW forcing changes are larger in case 2 than in case 1 (Figures 1d and 1e), which should induce stronger downward/upward circulation between 60–120 km thus larger temperature response in case 2, but such response is not seen in Figures 1d and 1e. This may be partly due to the larger air density at lower breaking levels in case 2. Second, although the vertical depth of GW forcing in the base case between January 24 and 28 above 80 km is wider than that in case 1 (Figures 1b and 1d), the overall vertical depths of the mesospheric cooling regions above 65 km are comparable in the two cases. These discrepancies cannot be explained by GW forcing alone but by the combinations of GW forcing and PW forcing in the MLT.

[10] Figure 3 shows the temperature anomalies along with vector plots of the changes of residual circulation (Figures 3a–3c), the changes of parameterized GW forcing (Figures 3d–3f), the changes of resolved PW forcing (the Eliassen–Palm flux divergence) (Figures 3g–3i), and the resolved PW perturbations in the zonal wind field (Figures 3j–3l). Here, the changes of GW and PW forcings and residual circulation are the differences between January 18 (before SSW) and January 25 (during SSW). The changes of residual circulation in Figures 3a–3c are driven by the Coriolis forces (shown as black arrows in Figures 3d–3i) induced by the changes of GW and PW forcings. As clearly seen in Figures 3a–3c, the locations of cooling/warming of temperature anomalies correspond well with the changes of the upward/downward circulation.

[11] Compared with case 1, eastward GW forcing in case 2 locates at lower heights at middle latitudes but at similar heights at high latitudes (Figures 3e and 3f). We

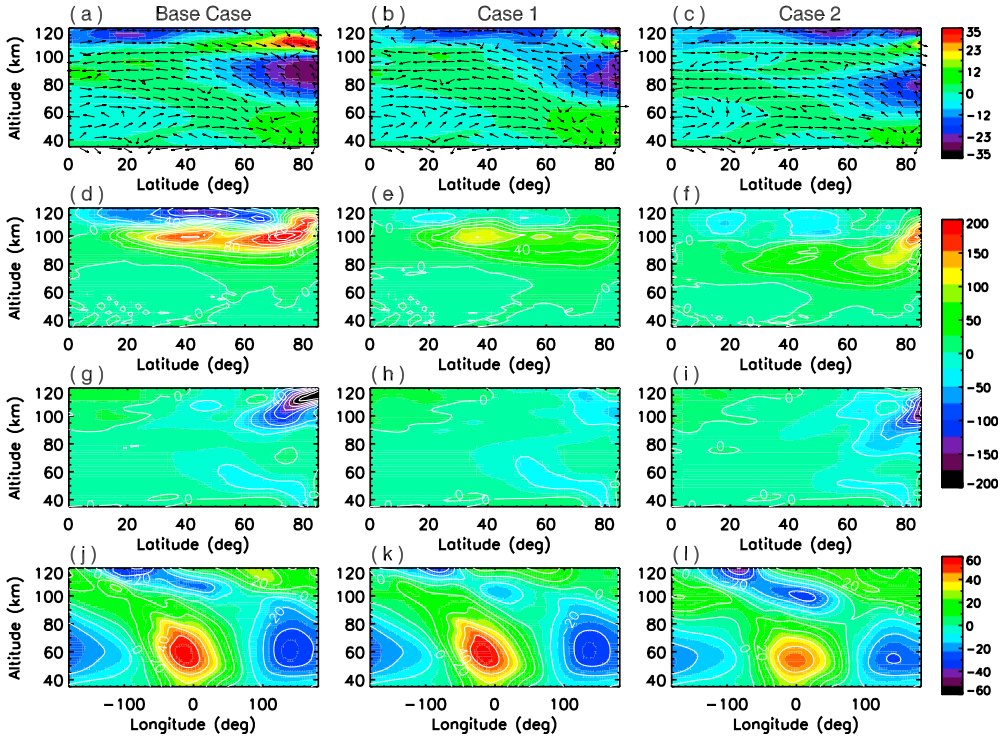

Figure 3. (a, b, c) The zonal-mean temperature anomalies from January 18 over-plotted with the changes of residual circulation, (d, e, f) the changes of parameterized GW forcing (m/s/day), (g, h, i) the changes of resolved PW forcing (m/s/day), and (j, k, l) the planetary scale perturbations on zonal wind (m/s) at 64°N on January 25 for three different cases (left: base case, middle: case 1, and right: case 2). The residual circulation vectors are normalized. Black arrows in Figures 3d–3i represent the Coriolis force induced by the corresponding forcing changes. Negative/positive value represents the westward/eastward forcing and zonal wind.

also notice that the high-latitude GW forcing in case 2 is much stronger than that in case 1. In the meantime, westward PW forcing in case 2 is significantly larger than that in case 1 (Figures 3h and 3i). The westward PW forcing in case 2 overlaps with eastward GW forcing at high latitudes. Thus, the PW forcing cancels the GW forcing in case 2, leading to the MLT temperature anomalies at high latitudes comparable to case 1. This explains the first exception mentioned above.

[12] The second exception, i.e., discrepancy in the vertical depth of the mesospheric cooling region in the base case and in case 1, is explained by the differences in downward flow at 100–120 km. In Figures 3d, 3e, 3g, and 3h, poleward circulation induced by combinations of westward GW and westward PW forcings between 100–120 km are larger in the base case than in case 1, leading to the stronger downward flow at 100–120 km in the base case. Such enhanced downward flow at 100–120 km erodes the region with upward flow induced by eastward GW forcing. In other words, the region of upward flow in the base case is shrunk by the strong downward flow above it. Thus, the vertical depth of cooling at 70–100 km in the base case is similar to that in case 1, even though the vertical depths of GW forcing regions are wider in the base case.

[13] The origin of PW in MLT is an interesting question. The PW forcing in Figures 3g–3i appears to be correlated with GW forcing in Figures 3d–3f. Both PW and GW forcing changes at high latitudes are over 150 m/s/day in the base case, but less than 50 m/s/day in case 1. Both PW and GW forcing regions are ~10 km lower in case 2 than in the base case. *Smith* [1996] suggests that the planetary-scale disturbances are generated in-situ by longitudinal variations of GW forcing in the mesosphere due to the GW filtering by PWs in the stratosphere. According to *Smith* [1996], if PWs in Figures 3g–3i are generated in-situ by the mesospheric GW forcing, the phases of PWs in the stratosphere and above the mesosphere are expected to be 180 degrees out of phase. Figures 3j–3l show the planetary scale perturbations on the zonal wind field, and the phases of PWs above 100 km are ~180 degrees out of phase from those below 100 km for all the cases. Thus, our study indicates that PWs contributing to the simulated MLT temperature anomalies are generated in-situ by GW forcing during the SSW.

4. Conclusions

[14] We examine how the height, vertical depth, and magnitude of the cooling and warming regions in the MLT vary with GW parameters in TIME-GCM during a minor SSW. All of the TIME-GCM simulations with and without GW parameterization show the stratospheric jet reversal, stratospheric warming, and mesospheric cooling. Thus, we confirm that the general features of SSWs in the stratosphere and the lower mesosphere are mainly determined by PWs as suggested by *Matsuno* [1971]. The height, vertical depth, and magnitude of the MLT cooling and warming regions, on the other hand, vary significantly with GW forcing.

[15] The characteristics of GW forcing are heavily dependent on the specifications of GW parameters in the model: GWs with wider spectral width produce the wider vertical extent of the GW forcing region, and GWs with shorter horizontal wavelengths and larger amplitudes result in the lower height of the GW forcing region. The GW forcing controls the pattern and strength of residual circulation and thereby the characteristics of the MLT cooling and warming regions. The height of the MLT cooling and warming regions is mainly determined by the height of GW breaking. The vertical depth and magnitude of the cooling and warming regions are closely tied to the vertical depth and magnitude of the GW forcing. Both of these features could be modified by PW forcing through influencing the residual circulation. Our simulations in the base case show that westward GW forcing at middle latitudes and PW forcing at high latitudes induce poleward flow in the lower thermosphere above the equatorward flow in the upper mesosphere generated by eastward GW forcing at high latitudes. This circulation drives the downward flow in the lower thermosphere and the upward flow in the upper mesosphere, leading to the adiabatic warming and cooling, respectively. Furthermore, the PW occurrence height can vary with GW breaking height, leading to the cancellation between PW and GW forcings. This could further modify the circulation thus the cooling and warming characteristics in the MLT. These PWs occurring at high latitudes in MLT are likely generated in-situ by GW forcing.

[16] Therefore, our study shows that the height, width, and magnitude of the MLT cooling and warming regions during SSWs are strongly affected by GWs directly through GW forcing and indirectly through the in-situ generation of PWs. Given the sensitivity of MLT response to GW parameters, uncertainties in GW parameters may be responsible for the discrepancy between model and observations. The variability of MLT temperature responses to different SSW events may also reflect the variability in GW source and propagation. Better knowledge of the GW source and propagation during SSWs is thus critical for correctly simulating the impacts of SSWs on MLT.

[17] **Acknowledgments.** We sincerely acknowledge Joseph Comeaux and Joseph McInerney for their help in TIME-GCM simulations and Adrian J. McDonald for his valuable comments. We thank the European Centre for Medium-Range Weather Forecasts (ECMWF) for providing data. C.Y. acknowledges the generous support of NCAR Newkirk Graduate Fellowship. H.L.L.'s effort is in part supported by the Office of Naval Research (N00014-07-C0209). X.C. and C.Y. were partially supported by NSF CAREER grant ATM-0645584. National Center for Atmospheric Research is sponsored by the National Science Foundation (NSF).

References

Coy, L., D. E. Siskind, S. D. Eckermann, J. P. McCormack, D. R. Allen, and T. F. Hogan (2005), Modeling the August 2002 minor warming event, *Geophys. Res. Lett.*, *32*, L07808, doi:10.1029/2005GL022400.

Holton, J. R. (1983), The influence of gravity wave breaking on the general circulation of the middle atmosphere, *J. Atmos. Sci.*, *40*, 2497–2507, doi:10.1175/1520-0469(1983)040<2497:TIOGWB>2.0.CO;2.

Labitzke, K. (1972), Temperature changes in the mesosphere and stratosphere connected with circulation changes in winter, *J. Atmos. Sci.*, *29*, 756–766, doi:10.1175/1520-0469(1972)029<0756:TCITMA>2.0.CO;2.

Lindzen, R. S. (1981), Turbulence and stress owing to gravity wave and tidal breakdown, *J. Geophys. Res.*, *86*, 9707–9714, doi:10.1029/JC086iC10p09707.

Liu, H.-L., and R. G. Roble (2002), A study of a self-generated stratospheric sudden warming and its mesospheric-lower thermospheric impacts using the coupled TIME-GCM/CCM3, *J. Geophys. Res.*, *107*(D23), 4695, doi:10.1029/2001JD001533.

Matsuno, T. (1971), A dynamical model of the sudden stratospheric warming, *J. Atmos. Sci.*, *28*, 1479–1494, doi:10.1175/1520-0469(1971)028<1479:ADMOTS>2.0.CO;2.

Ren, S., S. M. Polavarapu, and T. G. Shepherd (2008), Vertical propagation of information in a middle atmosphere data assimilation system by gravity-wave drag feedbacks, *Geophys. Res. Lett.*, *35*, L06804, doi:10.1029/2007GL032699.

Siskind, D. E., L. Coy, and P. Espy (2005), Observations of stratospheric warmings and mesospheric coolings by the TIMED SABER instrument, *Geophys. Res. Lett.*, *32*, L09804, doi:10.1029/2005GL022399.

Smith, A. K. (1996), Longitudinal variations in mesospheric winds: Evidence for gravity wave filtering by planetary waves, *J. Atmos. Sci.*, *53*, 1156–1173, doi:10.1175/1520-0469(1996)053<1156:LVIMWE>2.0.CO;2.

X. Chu and C. Yamashita, Cooperative Institute for Research in Environmental Sciences, University of Colorado at Boulder, Boulder, CO 80309-0216, USA. (chihoko.yamashita@colorado.edu)

H.-L. Liu, High Altitude Observatory, National Center for Atmospheric Research, Boulder, CO 80307-3000, USA.